Journal of Volcanology and Geothermal Research 474 (2026) 108624

Contents lists available at ScienceDirect

Journal of Volcanology and Geothermal Research

journal homepage: www.journals.elsevier.com/journal-of-volcanology-and-geothermal-research

Water volumes, heat flow, and solute discharge from Old Faithful Geyser eruptions, Yellowstone National Park, USA

Shaul Hurwitz [a,*], R. Blaine McCleskey [b], Maxwell L. Rudolph [c], Sara Peek [a], David A. Roth [b], Melissa Schott-Atkins [a,*], Michael Manga [d], Kiernan F. Folz Donahue [e], Mara H. Reed [d,e], Jefferson D.G. Hungerford [e]

[a] U.S. Geological Survey, Moffett Field, California, USA
[b] U.S. Geological Survey, Boulder, CO, USA
[c] Department of Earth and Planetary Sciences, University of California, Davis, California, USA
[d] Department of Earth and Planetary Science, University of California, Berkeley, California, USA
[e] Yellowstone Center for Resources, Yellowstone National Park, Wyoming, USA

A R T I C L E I N F O

Keywords:
Hydrothermal
Multiphase
Water discharge
Reservoir
Flume
Heat flow
Silica

A B S T R A C T

The iconic Old Faithful Geyser in Yellowstone National Park, USA, has attracted a significant amount of research because of the relative regularity and impressive size of its eruptions. Numerous studies have included observations, measurements, and analyses that informed models of geyser eruptions. However, fundamental quantities, including the associated mass and heat discharged, remain poorly constrained. In April 2025 we measured the volume of water from 45 Old Faithful Geyser eruptions using a portable flume in an outflow channel and specific conductance measurements in the Firehole River. We used high-speed video to perform velocimetry, measured changes in water chemistry to calculate the volume of water evaporated along the outflow channels, and used thermodynamic calculations to estimate the volume of water erupted as steam and to quantify the geyser's heat output. The calculated average volume of water discharged by Old Faithful Geyser in each eruption is 27.9 ± 9.4 m^3, with no relation between eruption volume and the length of the preceding eruption interval. Video analysis of the eruption's liquid-dominated phase yields similar volumes of 21–30 m^3. The calculated heat flow from the geyser is 2.2–2.4 MW and the average annual discharge of chloride, fluoride, and arsenic are 63 tons, 3.9 tons, and 241 kg, respectively. Average annual silica deposition rate on the geyser cone and along the outflow channels is 7 tons. This study provides a methodology for future studies at geysers worldwide and a baseline for monitoring future activity changes at Old Faithful.

1. Introduction

Natural geysers are rare. There are fewer than 1000 worldwide, with approximately half in Yellowstone National Park, USA (Bryan, 2008) (Fig. 1). The rarity of geysers reflects the special conditions needed for their formation: availability of water and heat, and a subsurface hydraulic architecture that has the right geometry of fractures and cavities to permit episodic discharge (Hurwitz and Manga, 2017). Their eruptions are driven by the conversion of thermal to kinetic energy during decompression of ascending waters. Geysers provide a unique natural laboratory to test hypotheses about volcanic eruptions, because they have many similarities to volcanoes, especially with regards to heat and mass flux, eruption dynamics, and seismicity (Kieffer, 1984, 2017). This has motivated scientists from multiple disciplines to study the complex processes associated with geyser eruptions; the geophysical signals that can be measured before, during, and after an eruption; and to form hypotheses regarding the occurrence and limits of life on Earth and elsewhere in the solar system (Hurwitz and Manga, 2017; Hurwitz et al., 2021). An improved understanding of geyser dynamics may yield insight into other multiphase episodic processes and other self-organized, intermittent processes in nature that result from localized input of energy and mass (Kieffer, 1989, 2017).

Old Faithful Geyser in the Upper Geyser Basin (UGB) of Yellowstone National Park (Fig. 1) was named by Ferdinand V. Hayden, who led the 1871 geological survey of northwestern Wyoming that resulted in the establishment of Yellowstone as the first U.S. National Park in 1872.

* Corresponding authors at: U.S. Geological Survey, Moffett Field, California, USA.
E-mail address: shaulh@usgs.gov (S. Hurwitz).

https://doi.org/10.1016/j.jvolgeores.2026.108624
Received 5 January 2026; Received in revised form 7 April 2026; Accepted 16 April 2026
Available online 17 April 2026

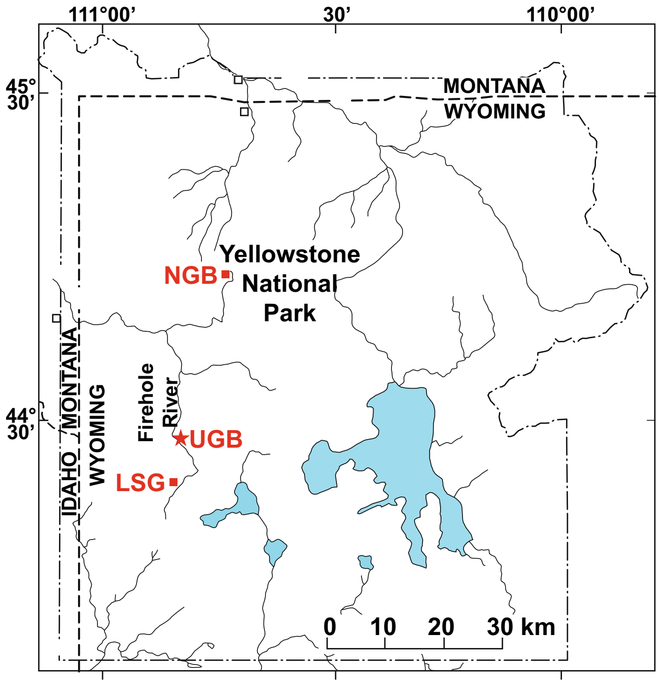

Fig. 1. Map of Yellowstone National Park showing state boundaries (dashed lines), park boundary (dash-dot line), major streams, the Upper Geyser Basin (UGB) in which Old Faithful Geyser is located, Norris Geyser Basin (NBG, symbol at the location of Steamboat Geyser), and Lone Star Geyser (LSG).

Hayden (1883) wrote: "*[Old Faithful] is so regular in its operations and they occur so frequently that it has afforded unusual facilities for observation*". Because of the relative regularity of its eruptions, the geyser has attracted a significant amount of research. Studies include temperature and pressure measurements (Birch and Kennedy, *1972*; Hutchinson et al., 1997; Kedar et al., 1998; Van Orstrand, 1924) and video observations (Hutchinson et al., 1997) in the conduit, analysis of seismicity associated with the eruption cycle and delineation of the subsurface structure (Cros et al., 2011; Hurwitz and Shelly, 2017; Kedar et al., 1996; Kedar et al., *1998*; Kieffer, *1984*; Nicholls and Rinehart, 1967; Rinehart, 1965, 1969; Vandemeulebrouck et al., 2013; Wu et al., 2017, 2019), statistical analysis of eruption intervals (Azzalini and Bowman, 1990; Nicholl et al., 1994; Vicari and Van Dorp, 2013) and their modulation in response to large regional earthquakes (Hurwitz et al., 2014), interaction with surrounding geysers (Fagan et al., 2022; Marler, 1951; Rojstaczer et al., 2003), and response to seasonal and inter-annual precipitation patterns (Hurwitz et al., 2008) and severe and prolonged droughts (Hurwitz et al., 2020). Studies have also documented the nearly constant chemical composition of erupted water for at least 130 years (Hurwitz et al., 2012a; Price et al., 2024), that most of the erupted water was recharged more than 70 years prior (Hurwitz et al., 2025) and ascends towards the geyser after flowing through the deep and hot 631.3 ± 4.3 ka Lava Creek Tuff (Matthews et al., 2015) and overlying rhyolites (Paces et al., 2024), and that deposits called "geyser eggs" form (Smith et al., 2018) and diverse microbes thrive in splash pools on the geyser cone (Keller et al., 2023). Finally, several physical models for the geyser's eruptions were formulated based on myriad measurements (Fournier, 1969; Geis Jr, 1966; Kieffer, 1989; O'Hara and Esawi, 2013; Rudolph and Sohn, 2017).

However, the volume of water erupted, and the associated mass and heat discharged from Old Faithful Geyser remain poorly constrained, despite being fundamental thermal and physical properties of erupting systems. Quantitative determination of these properties is important because it provides input to physical models of geyser eruptions and can serve as a baseline to better enable detection of changes resulting from earthquakes, climate variability, changes in subsurface heat, or infrastructure development (Foley et al., 2014; Hurwitz and Lowenstern, 2014). Measuring volume is challenging because the erupted water flows through several very shallow outflow channels (Fig. 2) and wind can carry water droplets away from these runoff channels, and because some of the erupted fluid is lost to evaporation and possibly also to recharge into the geyser's sinter deposits. Previous estimates of erupted volumes ranged from 20 m^3 (Kieffer, 1984) to 14–32 m^3 (Hutchinson et al., 1997), and 38–45 m^3 (Allen and Day, 1935). However, these studies did not provide details on the methods used, the number of flumes and the outflow channels in which they were deployed, the number of eruptions captured, and the weather during measurements. Thus, it is not possible to assess the uncertainty in these values and their reported ranges.

Between 11 and 15 April 2025, we measured and quantified the volume of water erupting from Old Faithful Geyser using a combination of methods, because the erupted water flows in different directions depending on the wind. The methods included measurements with a flume in the major outflow channel located to the west of the vent, specific conductance and water discharge measurements in the Firehole River, into which the geyser's channels drain (Fig. 2), and using high-speed video recordings to perform velocimetry. We use changes in water chemistry to calculate the volume of water evaporated along the geyser's outflow channels between the geyser cone and the discharge measurement locations, and thermodynamic calculations to estimate the mass of steam erupted and to calculate heat flow. Finally, we calculate the mass of major solutes discharged by the geyser. The results improve the understanding of how the most iconic geyser in the world operates and provides a baseline for tracking changes in the geyser's activity.

2. Old Faithful Geyser hydrology

The water erupted by Old Faithful Geyser (Fig. 3a) typically flows away from the vent in one or more of the six shallow channels (Fig. 2) depending on wind direction. These channels are generally only a few cm deeper than the surrounding siliceous sinter terrace and their width varies from a few cm to more than 1 m. Outflow channels 3–6 flow into the Firehole River ~170 m north of the geyser vent. Water flowing southward in channel number 1 is diverted by a culvert and then merges with channel number 2, which flows to an open meadow to the northwest, with no obvious channels leaving the meadow (Fig. 2). Thus, the total volume of liquid water flowing in the outflow channels is the sum of the discharge in channel number 1 and the volume that flows through channels number 3–6 into the Firehole River.

The silica sinter deposits lining the outflow channels within the terrace are of low permeability (Vitale et al., 2008) so that there is minimal seepage of water into the subsurface from the outflow channels and from rain and snow (Fig. 3b). This is supported by the lack of meteoric water tracers (stable water isotopes and tritium) in the water erupted from the geyser (Hurwitz et al., 2012a, 2025). Ground penetrating radar (GPR) data, combined with thermal infrared imaging near the geyser's cone, indicate some shallow subsurface fractures in the siliceous sinter, including a WNW-trending fracture on the cone itself (Jaworowski et al., 2020; Lynne et al., 2018). In channels where flow is relatively small following the eruption, water freezes during much of the year, and thaws only when larger volumes of erupting hot water flow through in the channel.

Video observations made in the conduit of Old Faithful Geyser in the summer of 1992 (https://www.youtube.com/watch?v=8luNCFUnvBw) to a depth of nearly 13 m (Hutchinson et al., 1997) reveal an irregular, elongated fissure-like channel with fractured walls lined with silica sinter. The conduit is a narrow slot at the surface that changes shape significantly with depth. At a depth of ~7 m below the surface, the slot narrows to ~11 cm, forming a constriction. A maximum temperature of 118 °C was measured in 1942 (Birch and Kennedy, *1972*) and again between 1983 and 1993 (Hutchinson et al., 1997) at a depth of 21.7 m. Short duration temperature spikes (5–10 s) of up to 129.5 °C were

Fig. 2. Aerial image of Old Faithful Geyser and its surroundings. The red numbered labels on white backgrounds refer to outflow channels. Water flowing southward in channel number 1 is diverted by a culvert and then merges with channel number 2, which then flows towards the flume and from there to an open meadow to the northwest. Outflow channels 3–6 flow into the Firehole River. Continuous specific conductance measurements and campaign sampling of water for chemical analysis were carried out upstream and downstream from where channels 3–6 enter the river. Continuous specific conductance measurements and samples were collected on the outflow channel of Beehive Geyser before it enters the Firehole River. Also shown are the locations from which video of the eruption jet was captured (V1-V3) and the location of the weather station (V1) deployed during the experiment in April 2025. (For interpretation of the references to colour in this figure legend, the reader is referred to the web version of this article.)

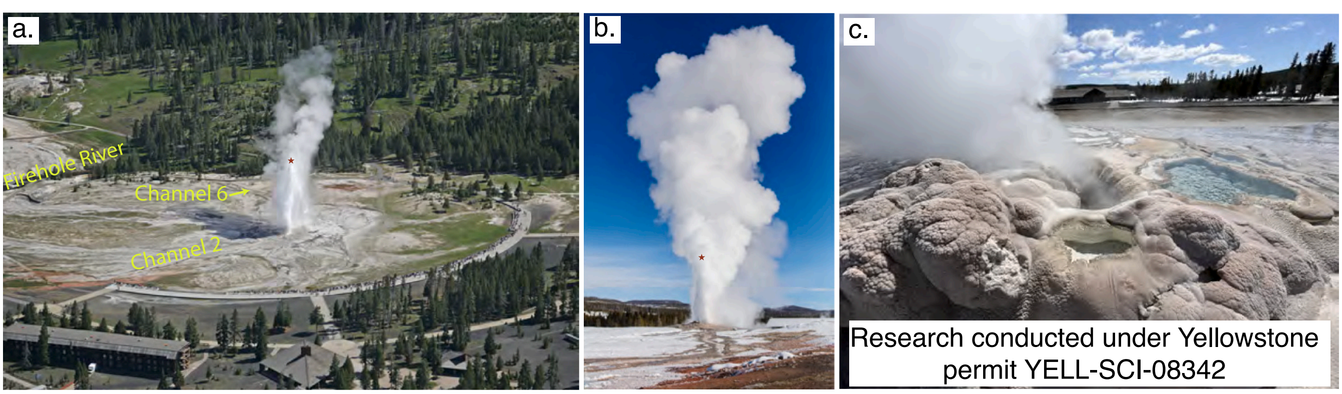

Fig. 3. a) Photo looking northeast showing an Old Faithful Geyser eruption on 22 June 2006. The red star denotes the approximate top of the liquid-dominated jet (photo by Jim Peaco, National Park Service). b) Photo looking northeast of Old Faithful Geyser erupting in the winter of 2017, with snow accumulating on the sinter terrace. The liquid jet (the red star denotes the approximate top) is limited in extent, and most of the plume consists of steam (photo by Jacob W. Frank, National Park Service). c) The Old Faithful Geyser vent and adjacent splash pool from where water samples were collected for chemical analysis immediately after an eruption. The width of the pool is approximately 1 m (photo by Shaul Hurwitz, U.S. Geological Survey). (For interpretation of the references to colour in this figure legend, the reader is referred to the web version of this article.)

measured a few times at the beginning of an eruption, suggesting that water from deeper than 21.7 m was involved (Hutchinson et al., 1997).

3. Methods

To determine the onset of the eruptions, we used daytime visual observations (geysertimes.org) supplemented by data from a National Park Service temperature logger located on the geyser mound at the head of channel number 2 (Fig. 2). Based on correlations between the temperature logger and the reported observations, we determined that the sharp temperature increase recorded by the logger lags the eruption onset by three minutes.

Detailed descriptions of the methods used to measure water discharge are provided in a U.S. Geological Survey (USGS) data release (McCleskey et al., 2026) and here we provide a summary. Between 12 and 15 April 2025, a USGS portable Parshall flume (Kilpatrick and Schneider, 1983; Parshall, 1950) was placed in the outflow channel number 2 drainage (Fig. 2). This location was chosen because it drains a significant fraction of the erupted water and because this was the only place we could channel all water through the flume without significant leakage or disturbance to the sinter deposits. The Parshall flume was used because it allows for flow measurements by continuously monitoring of water level in the channel. Discharge measurements with a current meter were not used because the depth of the channel is too shallow, velocities are too low, and measurements take too long to capture the transient flow from the eruptions. The flume was leveled both laterally and along its longitudinal axis, and sandbags were placed to prevent leakage under and around it (Fig. 4). To continuously measure stage, a factory-calibrated vented pressure transducer (Level TROLL 700, In-Situ Inc.) with a pressure range of 0 to 5 pounds per square inch (0–34.5 kPa) was inserted in a stilling well that was hydraulically connected to the flume by a 3/8-in. (0.95-cm) hole. A 6 ft (1.8 m) vented cable with a desiccant at the end was attached to the transducer to prevent water from entering. The height of the water in the stilling well was sampled every 10 s. Since the stilling well base is below the base of the flume, we calculated the hydraulic head by subtracting 4.6 cm from the depth measurement of the transducer.

A best-fit curve through the hydraulic head-discharge relation for the flume was determined. To obtain the volume of an individual eruption, we summed all the readings for each 10-s measurement, from when values increased above the baseline until the values returned to the baseline. The time that it took the water slug to arrive at the flume following the onset of an eruption ranged between 6 and 15 min, with an average and median of 9 min. In a few cases, the volume of water exceeded the capacity of the flume (Fig. 5). For individual readings that attained the maximum height in the well, we added 10%. However, a 5% or 15% correction resulted in volume changes that are within the uncertainties of the measurements.

To validate the pressure-transducer measurements, in the flume's stilling well we collocated a 12-in. (30.5 cm) calibrated liquid-level electronic solid-state sensor with a resistive output that varies with the level of the fluid (*eTape* Liquid Level Sensor by Adafruit) for 13 daytime eruptions. The sensor's plastic envelope is compressed by the hydrostatic pressure of the fluid in which it is immersed. The resulting change in resistance corresponds to the distance from the top of the sensor to the surface of the fluid. The sensor's resistive output, which is inversely proportional to the height of the liquid, was calibrated in the laboratory. Measurements were made every 10 s to temporally align with the transducer measurements and were recorded on a datalogger ((Campbell Scientific Inc.).

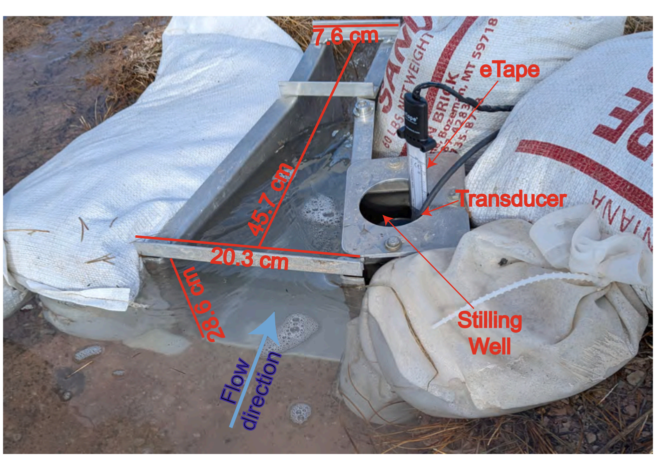

Fig. 4. Photo of the portable Parshall flume placed in outflow channel number 2 (Fig. 2). Sandbags were placed to channel the water into the flume and prevent flow under and around it. A vented pressure transducer and a liquid level electronic solid-state sensor with a resistive output (eTape) were inserted in the small stilling well that is hydraulically connected to the flume by a small hole. The study was conducted under research permit YELL-SCI- 08342.

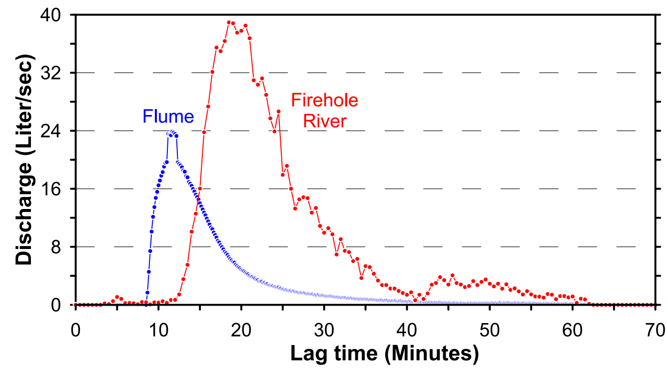

Fig. 5. An example of continuous water discharge measurements for water flowing in outflow channels 1 and 2 through the flume and in outflow channels 3–6 to the Firehole River (based on specific conductance) (Fig. 2). This eruption (number 24), which was the most voluminous measured, started on 14 April 2025 at 14:36 Mountain Standard Time.

To measure the volume of erupted water (V_G) that flows into the Firehole River through channels 3–6 (Fig. 2), we follow a modified method described in McCleskey et al. (2025) for slug addition and continuous downstream measurement of specific conductance where V_G (L) is determined by:

$$V_G = Q_U \int_0^T \frac{(SC_D - SC_U)}{(SC_G - SC_D)}(t)dt \tag{1}$$

and Q_U is the river discharge ($L \cdot s^{-1}$) upstream of outflow channels, SC is specific conductance (μS/cm; subscripts G, U, and D, are for geyser, upstream, and downstream, respectively), dt is the time difference (s) between SC measurements, and T is the time at which the river concentration returns to background. The SC_D and SC_U were measured with a sensor (In-Situ Aqua Troll 100) programmed to log SC measurements every 30 s. The continuous discharge of the Firehole River (Q_U) was approximated by adding 10 L/s (or $<$ 1% of the total discharge) to measured values obtained from the U.S. Geological Survey gage on the Firehole River at Old Faithful, YNP (station 06036805; U.S. Geological Survey, 2022) where discharge is measured every 15 min. These estimates were based on several downstream discrete measurements. The SC_G (1808 μS/cm) was determined from erupted water measured in the splash pool on the Old Faithful cone (Fig. 3c). Since the slug addition method depends on the mass of solute entering the river (McCleskey et al., 2025) and since the erupted volume of water is very small compared to the water discharge in the river, eq. (1) used the specific conductance of erupted water at the source (splash pool shown in Fig. 3c). Evaporation of the water flowing into the river is minor and not accounted for. Specific conductance measurements in the Firehole River were made downstream from the Beehive Geyser outflow channel (Fig. 2) and therefore, we also measured specific conductance at the bottom of the Beehive Geyser outflow channel, before it merges into the Firehole River. During the experiment, slugs of water from the relatively infrequent Beehive Geyser eruptions, the only other significant input of thermal water along the path between Old Faithful's runoff channel and the downstream specific-conductance measurements, did not overlap with water slugs from Old Faithful Geyser eruptions.

A weather station (Campbell Scientific Inc.) was set up to the southeast of Old Faithful Geyser for the duration of the discharge measurement experiment (Fig. 2). The weather station was equipped with a temperature sensor, a barometer, a tipping bucket rain gauge, and an anemometer for measuring wind direction and speed. Air temperature, pressure, and rain accumulation were sampled every 5 s, with the average of those measurements recorded at 5-min intervals. Average wind speed and direction were also sampled every 5 s, with average values recorded at 1-min intervals.

To measure the velocity of the erupting plume, images were captured with a high-speed camera (Phantom C321, https://www.phantomhighspeed.com/) that has a color sensor with a resolution of 1920 × 1080 pixels. We captured and successfully processed videos of two eruptions on 11 April 2025, from location V1 (Fig. 2) and one on 13 April from location V3. Jet imaging with the high-speed camera on April 11 did not coincide with the flume and river specific-conductance measurements, but a direct comparison can be made for the eruption on April 13. Videos were recorded at 100–120 frames per second (fps) with exposure durations of 100–400 μsec, depending on framerate and lighting. The location of the camera (Fig. 2) was chosen to provide an unobstructed view of the jet while minimizing the presence of obscuring steam, with consideration for the direction of lighting. Many of the acquired videos were unsuitable for velocity measurement due to changing lighting conditions and condensed steam obscuring the jet.

4. Results

4.1. Flume and river measurements

We measured water volumes from 45 geyser eruptions for which the average interval between eruptions was 93 min, with a minimum of 58 min and a maximum of 140 min. We measured water discharge from outflow channels 1 and 2 using the Parshall flume (Fig. 4) and water discharge from outflow channels 3–6 by measuring specific conductance in the Firehole River (Fig. 2). For 12 of the 13 eruptions in which the height of the water in the flume's stilling well was measured by both the pressure transducer and the eTape, differences for all 10-s measurements were within 10%. Data are provided in a U.S. Geological Survey data release (McCleskey et al., 2026).

It took between 6 and 15 min, with an average and median of 9 min from the onset of the eruption, until the water slug arrived at the flume, and between 11 and 46 min, with average and a median of 18 min, from the onset of the eruption until the sharp increase in specific conductance (Fig. 5) at the downstream station in the Firehole River (Fig. 2). During some of the eruptions there was ice accumulating in the channels. This ice thawed either when air temperature increased sufficiently or when hot water from eruptions was flowing. There were no visual observations of significant amounts of ice accumulating in channels 1, 2, and 6 (Fig. 2) which drained most of the water from the eruptions.

There is no evidence that previous estimates of erupted volume from Old Faithful Geyser (Allen and Day, 1935; Hutchinson et al., *1997*; Kieffer, 1984) accounted for the volume of water lost by evaporation between the geyser cone and the location of discharge measurements. Similarly, previous water discharge measurements made at Lone Star and Steamboat (Norris Geyser Basin) Geysers (Fig. 1) did not account for water evaporated between the geyser and the location of discharge measurements (Karlstrom et al., 2013; Reed et al., 2021). At Steamboat Geyser, water discharge was measured ~2.2 km downstream from the geyser, potentially leading to substantial underestimation of erupted volumes.

Some of the erupted water does evaporate along the outflow channels upstream of the locations of discharge measurements. A specific conductance probe located at the end of outflow channel 6, intended to provide information on the evaporated volume, provided unreliable data, likely because it was not submerged in water and did not thermally equilibrate during most eruptions. However, the specific conductance measurements in the Firehole River account for the volume of water evaporated in channels 3–6 because they are based on the mass of solutes from a slug. To quantify the volume of water evaporated in channels flowing to the flume (channels 1 & 2), we compare the concentrations of chloride, a conservative solute in magma-hydrothermal systems (Fournier, 1979b), in water at the end of the outflow channels with those in water in the splash pool on the geyser cone.

The total volume of erupted water (V_T) flowing through the flume, including the volume of water evaporated along channels 1 and 2 (Table S1), is calculated by considering changes in chloride concentrations between the splash pool and the location of the flume, and is given by:

$$V_T = V_F\,[Cl]_F/[Cl]_P \quad (2)$$

where subscripts F and P are for the flume and splash pool, respectively. The median and average chloride concentrations for 12 samples collected from the outflow channels during different times of the year between April 2007 and September 2008 (Hurwitz et al., 2012a), a sample collected in April 2025 (McCleskey et al., 2026), and 4 samples collected during 2 eruptions on June 26 and July 12, 2025, are 492 and 511 mg·L^{-1}, respectively (Table S2). Chloride concentrations ranged between 434 and 629 mg·L^{-1}, with samples collected during summer months having higher concentrations. The median chloride concentration of five samples collected from the splash pool between September 2021 and July 2025 is 424 mg·L^{-1}. Using the median concentrations in the outflow channels and in the splash pool, the multiplier in eq. 2 has a value of 1.15 (Table 2). Thus, all the volumes calculated based on discharge measurements at the flume were multiplied by 1.15, though there are likely large temporal variations in the degree of evaporation along the channels in response to changes in wind speed, air temperature, humidity, and travel time.

There was a large variability in the fraction of water flowing towards the flume through channel number 2 versus water flowing to the river through channels 3–6 which was only slightly correlated with wind speed and direction (Fig. 6). The minimum and maximum volumes of water flowing through the flume and to the river were 12.8 and 44.3 m^3, respectively (Table S1). The median volume was 27.8 m^3, the average was 26.3 m^3, and the standard deviation was 9.4 m^3 (Table 1; Fig. 7). The measured volumes of water for each eruption are provided in the Supplementary Material (Table S1). There was no relation between the eruption volumes and the preceding eruption intervals, but short eruptions defined as eruptions lasting less than 2.5 min) resulted in smaller volumes (Fig. 8) than long eruptions (typically greater than 3 min). There is also no relation between the erupted volume and the following eruption interval.

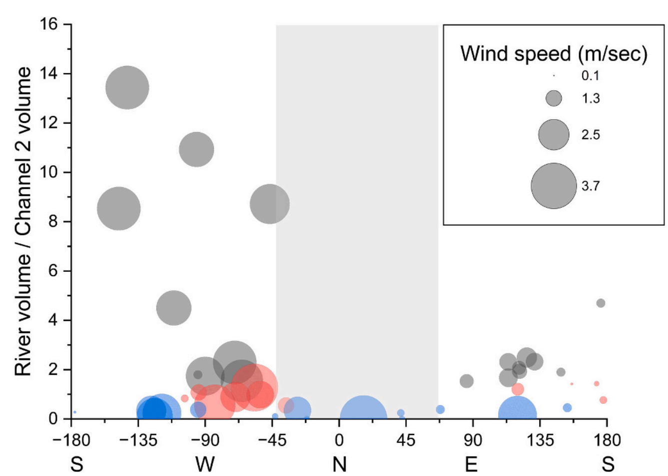

Fig. 6. The ratio of water volume flowing towards the Firehole River over the water volume flowing through the flume (Fig. 2) as a function of wind speed (circle size) and direction (x-axis). The blue circles with y-axis values of less than 0.5 represent eruptions where most water was flowing through the flume, whereas the gray circles (>1.5) represent eruptions where most water was flowing towards the river. The red circles represent eruptions where there was substantial flow both to the flume and to the river (0.5–1.5). The shaded gray rectangle represents the range of azimuths in which the wind was expected to cause the water to flow towards the flume (winds predominantly from the north). (For interpretation of the references to color in this figure legend, the reader is referred to the web version of this article.)

Table 1
Measured and calculated volumes of water (m^3) from Old Faithful.

Geyser eruptions	
Flume + river (liquid water)	
Minimum	12.8
Maximum	44.3
Median	27.8
Average	26.3
STDEV[1]	9.4
Steam[2]	
Average	1.5
STDEV	0.4
Total volume	**27.9**
STDEV	**9.4**

1- One standard deviation
2 - Initially liquid water erupted as steam

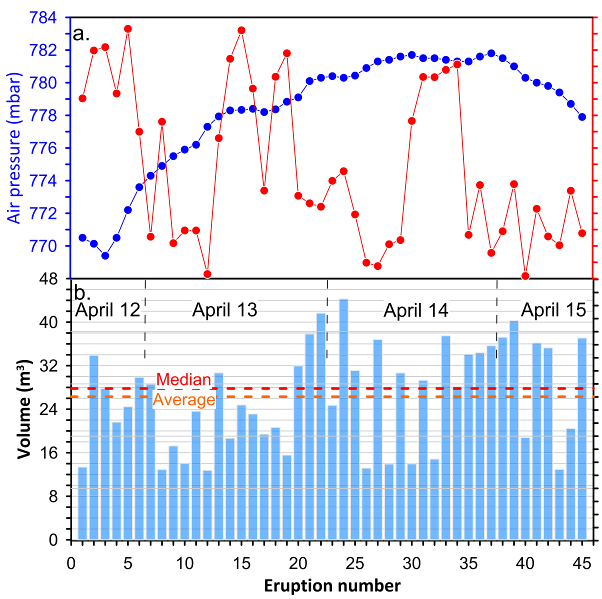

Fig. 7. a) Average air pressure (left axis and blue symbols and line) and wind speed (right axis and red symbols and line) during each of the 45 eruptions in April 2025. b) The combined volume of water flowing through outflow channels 3–6 (Fig. 2) to the Firehole River and water flowing through outflow channels number 1–2 to the flume. (For interpretation of the references to colour in this figure legend, the reader is referred to the web version of this article.)

4.2. Video measurements

The video data used for image analysis are available on Zenodo (Rudolph, 2026). We measured jet velocities using image correlation analysis in MATLAB (The MathWorks Inc, 2025). From the high-speed video recording, we constructed a streak image (called a kymograph) (Fig. 9a) of a (vertical) column of pixels centered on the geyser's jet vs. time. From the kymograph, we first segment the image to isolate the jet. Then, we analyze overlapping temporal windows of 100 frames. For each window, we compute the cross-correlation between rows of pixels. We use a peak-finding algorithm (MATLAB findpeaks, The MathWorks Inc, 2025) to identify the temporal lag at which the cross-correlation is maximized, retaining only lags that correspond to correlations over a threshold value to reject noise. We compute velocities from the change in height above the vent divided by temporal lag. Velocities measured above the vent are converted to exit velocities by assuming a ballistic trajectory. The jet height computed using image segmentation provides an independent means to validate the velocities computed by image correlation analysis, and the two methods yield very similar estimates of exit velocity and discharge (Fig. 9).

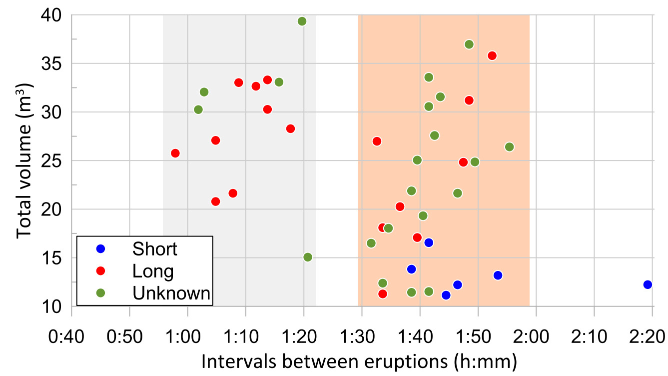

Fig. 8. Total volume of water erupted as a function of the preceding Old Faithful Geyser eruption intervals. The colors represent short (minor) and long (major) eruptions in the GeyserTimes.org eruption catalog. The green circles are from eruptions that lack observations, mostly during the night. (For interpretation of the references to colour in this figure legend, the reader is referred to the web version of this article.)

The high-speed video recordings of the geyser's eruptions document episodes of pre-play (minor splashing), a vigorous fountaining phase, and a protracted lower-height phase. A single eruption of Old Faithful along with our analyses of velocity and discharge are presented in Fig. 9. Eruptions are typically preceded by several episodes of pre-play, seen prior to 20s in Fig. 9a. The onset of the eruption, referred to as "initiation and unsteady flow" in Kieffer (1989), is characterized by growing pulses of discharge and the rise of the geyser's jet to ~28 m above the vent. Once the eruption is underway, the main phase is characterized by a steadier jet height, though some unsteadiness is still apparent in the flow. The velocities and cumulative discharge estimated during the 3-min period shown in Fig. 9, which represents a lower bound on the total volume of this eruption, is 30 ± 13 m^3. In addition to the eruption shown in Fig. 10, we measured discharge for two additional eruptions. The first eruption was a 'short' eruption with a smaller erupted volume of 21 ± 9 m^3 and a maximum jet height of 29 m. The second, for eruption 17 on April 13, 2025, yielded a volume of 28 ± 12 m^3. For this eruption, no maximum jet height could be measured due to the camera position. Erupted volume estimates based on jet height alone and based on image correlation are remarkably similar, differing by less than 10%.

5. Discussion

The hydrothermal system of the Yellowstone Plateau Volcanic Field (Christiansen, 2001) comprises more than 10,000 thermal features, including fumaroles, mud pots, thermal springs, hydrothermal explosion craters and geysers (Hurwitz and Lowenstern, 2014; Lowenstern and Hurwitz, 2008). Old Faithful Geyser in particular has attracted a significant amount of research. To provide input to physical models of geyser eruptions and to establish a baseline that can better enable detection of changes in geyser activity, we measured the volume of water discharged from 45 eruptions by combining measurements of water discharge from the geyser's southern outflow channels with a portable Parshall flume and from the northern outflow channels with specific conductance measurements in the Firehole River into which the geyser flows. We augment these measurements with measurements and calculations of water volume evaporated along the outflow channels between the geyser cone and the location of discharge measurements. We also analyzed images captured with a video camera to measure the volume of erupted water.

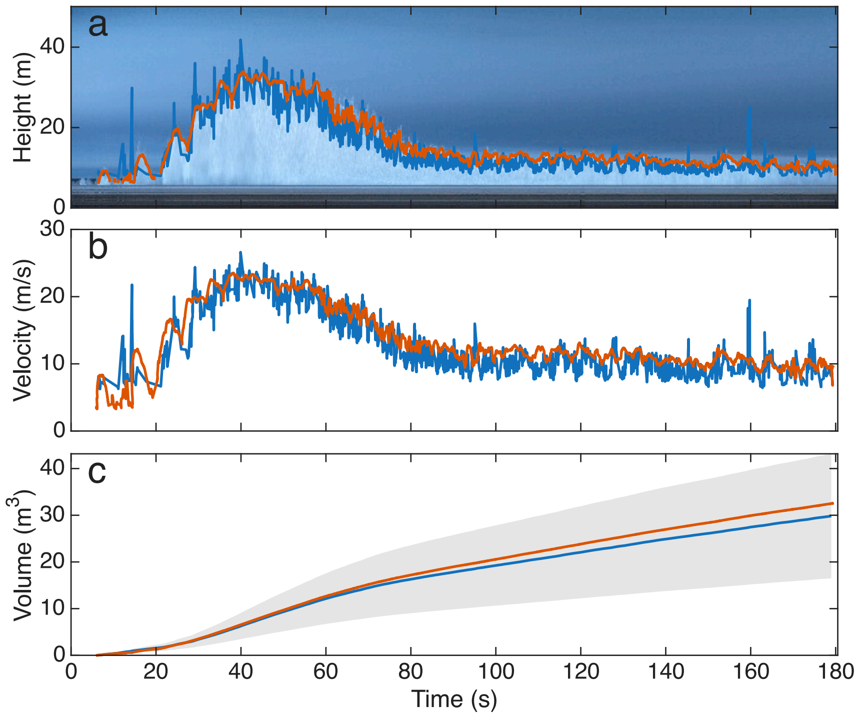

Fig. 9. a) Streak image (kymograph) for a single eruption of Old Faithful Geyser. The red curve delineates the boundary of the jet identified using image segmentation. The blue curve is the equivalent jet height measured using image correlation velocimetry. b) The exit velocity was computed using both methods, using the images and the jet height. c) The cumulative erupted volume computed using both methods. Here we assume a cross-sectional area of 0.69 m^2 and a fluid density of 20 kg·m^{-3}. The gray shaded region in c) indicates a confidence interval of 44%, discussed in the text. (For interpretation of the references to colour in this figure legend, the reader is referred to the web version of this article.)

5.1. Conceptual model for water and heat ascent from depth

We present a model for hot groundwater ascending from a reservoir at depth, through the immediate geyser reservoir ("bubble trap"), to the geyser vent, and eruption to atmosphere (Fig. 10). We assume that water is continuously decompressed adiabatically from the deeper reservoir where it has chemically and thermally equilibrated with the host rock. During ascent, decompression causes the water to boil, generating steam that condenses in the bubble trap. The assumption of adiabatic decompression means that no heat is exchanged between the ascending water and the surroundings rocks. We further assume that decompression is isentropic (rather than isenthalpic) as commonly assumed in models of geyser and volcano eruption dynamics for a compressible fluid (Kieffer, 1989; Lu and Kieffer, 2009; Mastin, 1995; Reed et al., 2021; Thiery and Mercury, 2009). This assumption implies that the expansion and acceleration of the ascending multiphase fluid is not significantly dissipated as heat by internal shearing or friction. Ascent of a multiphase fluid is consistent with results of seismic imaging that suggest hydrothermal flow to depths of at least 120 m (Wu et al., 2017) and vertical migration of seismic tremor from depths of at least 80 m to the shallow "bubble trap" within the eruption cycle (Wu et al., 2019).

To calculate the temperature of chemical equilibrium in the deep reservoir, we use the quartz adiabatic geothermometer which is based on the concentration of dissolved SiO_2 in the water (Fournier, 1977) and assumes that waters attained chemical equilibrium with quartz at the reservoir temperature, and that rates of quartz thermal equilibration with the thermal water are much faster than rates of conductive cooling to the host rock. We also assume that the short storage of water in the bubble trap did not cause chemical re-equilibration of the water or significant conductive cooling. We do not consider the effects of dissolved gas (mainly CO_2) which alter fluid properties and phase distribution (Hurwitz et al., 2016). The temperature dependence of quartz solubility in water is given by (Fournier and Potter II, *1982*):

$$T_{\mathrm{Quartz}}(^{\circ}\mathrm{C}) = (1522/(5.75\text{–}\log[\mathrm{SiO_2}])) - 273.15 \tag{3}$$

where T is in degrees Celsius. The average SiO_2 concentration of the five samples collected at the splash pool on the geyser cone (Fig. 3c) is 349 ± 25 mg·L^{-1} (Table 2). The resulting average temperature of 201 ± 5 °C is similar to previous estimates of 205 °C (Fournier, 1969) and 204 ± 4 °C (Hurwitz et al., 2012a). The Na/K geothermometer yields an unrealistically low reservoir temperature of 168 ± 3 °C using the equation in Fournier (1979a) and 186 ± 3 °C using the equation in Giggenbach (1988). The quartz conductive geothermometer with no steam loss (Fournier, 1977) yields a temperature of 221 ± 6 °C, but its application is unrealistic for this boiling system. Uncertainties associated with chemical geothermometer determinations suggest that the calculated reservoir temperatures in Yellowstone's geyser basins could differ by up to 15 °C (Cullen et al., 2019; King et al., 2016). The calculated reservoir temperature we adopt here is consistent with a temperature of 180 °C measured at a depth of 124 m in a borehole drilled in 1929 (later named C-1), 470 m to the southwest of Old Faithful Geyser (Fenner, 1936).

Based on tracking hydrothermal tremor sources (Wu et al., 2019), the transport of heat and water from the deep reservoir to the bubble trap, which acts as a condenser, is nearly continuous. A significant amount of the thermal energy flowing into the bubble trap is converted into kinetic energy driving the episodic (every ~93 min in April 2025) eruptions. At the onset of an eruption, the plume is liquid-dominated, and as the pressure in the bubble trap decreases, steam is formed. Steam is emitted from the geyser conduit until the vapor pressure is lower than the ambient atmospheric pressure.

5.2. Mass fraction of steam

Old Faithful geyser eruptions start with 1.5 to 3 min of a liquid-dominated phase that transitions to a longer steam-dominated phase typically lasting for up to 5 min. To quantify the total volume of erupted

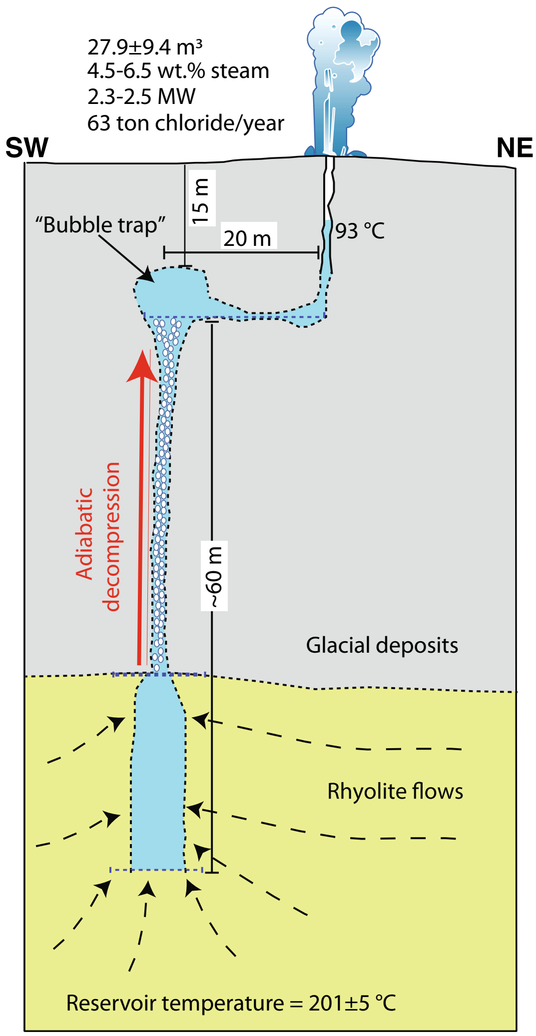

Fig. 10. Schematic illustration of water ascent from the deep hydrothermal reservoir, through the immediate reservoir ("bubble trap") and the conduit of Old Faithful Geyser. Water ascends by adiabatic decompression from a reservoir with a temperature of 201 ± 5 °C and the formation of steam bubbles that condense in the bubble trap prior to an eruption. The temperature of the erupting water is 93 °C. Modified after Wu et al. (2019).

Table 2
Concentrations of chloride (Cl) and silica (SiO_2) used for calculating the volumes of water evaporated along the Old Faithful Geyser outflow channels and the mass of annual silica deposition.

Location	Cl	SiO_2	Cl/Cl_c^1	SiO_2/SiO_2^2	SiO_2
	mg/L	mg/L			Ton/yr
Geyser Cone	424	354	(–)	(–)	(–)
Outflow channel	486	356	1.15	1.0	7

1 - Mass ratio of Cl concentration in the outflow channel to the concentration in the splash pool on the geyser cone used in equation number 2.
2 - Mass ratio of SiO_2 concentration in the outflow channel to the concentration in the splash pool on the geyser cone.
3 - Annual average mass of silica deposited between the geyser cone and discharge measurements.

water, it is necessary to include the volume that erupted as steam, which is difficult to measure directly. Although the "bubble trap" concept inherently involves the accumulation of vapor bubbles in the subsurface reservoir prior to eruption, the mass fraction of vapor is very small (in contrast to the volume fraction). Thus, to quantify the mass fraction of steam erupted, we assume that prior to the eruption, all the water in the bubble trap directly supplying the eruption was liquid.

To calculate the pre-eruptive volume in the bubble trap, we assume that the maximum temperatures measured at 21.7 m depth in the geyser conduit of 118 °C, with spikes of up to 129.5 °C (Birch and Kennedy, 1972; Hutchinson et al., 1997), represent the pre-eruptive temperature in the immediate reservoir ("bubble trap"). We further assume that, during the eruption, isentropic decompression of water from the reservoir generates liquid and steam that are emitted to the atmosphere at the boiling temperature for the local elevation (~93 °C). We calculate the mass fraction of steam that forms by isentropic decompression from 130 °C and from 118 °C using an energy balance given by:

$$S_{l-r} = x \cdot S_{v-a} + (1 - x) \cdot S_{l-a} \tag{4}$$

where S is entropy, x is vapor mass fraction, the subscripts l and v indicate liquid and vapor, and the subscripts r and a indicate reservoir and atmosphere conditions, respectively. We obtain the thermodynamic properties of pure water from the U.S. National Institute of Standards and Technology Thermophysical Properties of Fluid Systems database (NIST Standard Reference Database Number 69, 2025). Isentropic decompression from 130 and 118 °C to 93 °C results in steam mass fractions of 6.5 and 4.5%, respectively.

To calculate the mass of liquid water erupted as steam, we first multiply the average volume of water measured at the river and flume (26.3 m^3) by liquid water density at the eruption temperature of 93 °C (963.3 $kg \cdot m^{-3}$). We then divide it by the mass fraction of liquid (0.935–0.955) and multiply this value by the fraction erupted as steam, 0.065 and 0.045 for decompression from 130 and 118 to 93 °C, respectively. This results in steam masses of 1763 and 1195 kg per eruption. To convert to liquid volume, we multiply the erupted mass by liquid water density at 93 °C (963 $kg \cdot m^{-3}$) and determine volumes of 1.8 and 1.2 m^3 (4.6–6.8% of the liquid water volume).

5.3. Eruption intervals and water volumes

Despite Old Faithful's name, which implies that intervals between eruption are relatively constant, the intervals between the 45 eruptions in which water discharge was measured varied between 58 and 140 min, with a median and average of 99 and 93 min, respectively. The average interval is similar to the eruption intervals observed between 2001 and 2011 (90–93 min; Hurwitz et al., 2014) and slightly shorter than the 94.7 min observed during the year preceding the experiment (12 April 2024, to 11 April 2025) (GeyserTimes.org). Old Faithful Geyser eruption intervals increased significantly following large regional earthquakes in 1959 (M-7.3 Hebgen Lake, Montana), 1975 (M-6.1 near Norris Geyser Basin), and 1983 (M-6.9 Borah Peak, Idaho) (Hurwitz et al., 2014). Information on associated changes in erupted volumes is not available, though sustained regional droughts in the 13th and 14th centuries caused the geyser to stop erupting (Hurwitz et al., 2020).

We combine the volumes measured at the Firehole River and at the flume (26.3 ± 9.4 m^3) and the volume erupted as steam (1.5 ± 0.4 m^3) to calculate a total erupted water volume of 27.9 ± 9.4 m^3 (Table 1). This value is less than the values reported in Allen and Day (1935) of 38–45 m^3 and on the higher end of those reported by Hutchinson et al. (1997) of 14–32 m^3; however, those studies did not account for the volumes of water evaporated along the outflow channels and water erupting as steam.

Previous geyser experiments have used either high-speed or infrared cameras to obtain information on various aspects of geyser eruptions (Eibl et al., 2021, 2024; Karlstrom et al., 2013; Munoz-Saez et al., 2015; Teshima and Nishimura, 2024), but none have used video data to determine eruption volumes. Despite the large uncertainties in estimates from our video recordings of the liquid-dominated phase, the calculated volumes are within range of those made with the flume and riverine specific-conductance measurements. The camera observations also provide constraints on the dynamics of the erupting jet, which in turn inform eruption volume estimates by accounting for the fraction of steam in the liquid-dominated phase.

Velocities determined from video analysis of the liquid-dominated phase were compared with the imaged height of the jet, noting that for a ballistic trajectory without air resistance jet height h and velocity v are related through $v^2 = 2gh$. By assuming that the maximum velocity recorded is representative of the equilibrium sound speed in the fluid (Karlstrom et al., 2013; Lu and Kieffer, 2009), we can compute the mass fraction of steam and the density of the liquid-steam mixture. For example, assuming an ambient pressure of 750 mbar (75 kPa) and a maximum velocity (sound speed) of 25 $m \cdot sec^{-1}$, the corresponding mass fraction of steam is 1.5% and the density is 29.2 $kg \cdot m^{-3}$. If ballistic acceleration of the fluid begins at the base of the conduit (~20 m below the vent), the maximum velocity is 32 m/s, corresponding to a steam mass fraction of 2% and a density of 22.3 kg/m^3. On the other hand, as shown above, isentropic decompression of fluid from saturation conditions in the shallow reservoir (118–130 °C) would generate 4.5–6.5% steam (Section 5.2), and the density is 7.8–10.5 $kg \cdot m^{-3}$. Thus, there is considerable uncertainty (~50%) about the fluid density at the vent. We used an intermediate value of density (20.2 $kg \cdot m^{-3}$) to compute mass discharge and converted it to an equivalent volume of liquid water. The cross-sectional area of the vent was taken to be 0.7 m^2 based on observations within the conduit (Hutchinson et al., 1997; Kieffer, 1989). Because the discharge is proportional to cross-sectional area and fluid density, the large uncertainties in water density at the exit plane and in the exit plane cross-sectional area lead to a correspondingly large uncertainty in water discharge.

For a constant input of heat and water, it might be reasonably expected that the volume of erupted water should correlate with the length of the preceding intervals. However, at Old Faithful Geyser (Fig. 8) and Steamboat Geyser (in Norris Geyser Basin, Fig. 1), such correlations were not observed. The previously observed lack of correlation at Steamboat Geyser was explained by unsteady heat and mass discharge (Reed et al., 2021). Alternative, or complementary, explanations are: 1) large variation in the mass erupted as steam; 2) evaporation along the outflow channels, and ice accumulation in the channels that affected water-volume measurements; 3) the heat and mass input are not constant but depend on water levels in the geyser system, and 4) insufficient observations of eruption duration. The duration of an eruption interval depends on the duration of the preceding eruption, such that shorter eruptions are followed by shorter intervals and longer eruptions by longer intervals. Thus, the distribution of intervals is the same as the distribution of eruption durations. We found no apparent correlation between the average wind speed and the measured volumes of individual eruptions (Fig. 7), in contrast to the findings at Steamboat Geyser (Reed et al., 2021).

The calculated volumes of water erupting from Old Faithful Geyser that we report are larger than the volume of the reservoir ("bubble trap") estimated by Kieffer (1984) of 21.1 m^3 but are smaller than the bubble-trap volume estimated by Vandemeulebrouck et al. (2013) of ~62 m^3 which is based on more data. If we assume a reservoir with a volume of 62 m^3 full of liquid water prior to an eruption, our estimates of total volume erupted imply that approximately half of the reservoir is emptied by the end of an eruption. Partial emptying of the reservoir is consistent with the results of a tracer test where more than 24 consecutive eruptions were required to clear the geyser of an introduced dye (Fournier, 1969). They are also consistent with various other observations which imply that the volumes of geyser reservoirs and fracture complexes are significantly larger than the volumes of water discharged during a single eruption (Ardid et al., 2019; Hurwitz and Manga, 2017).

Water-discharge measurements have been made at other erupting geysers in Yellowstone National Park, but evaporative water loss along the outflow channels and the volume erupted as steam were not included in the final volume estimates. Thus, the reported volumes were likely somewhat underestimated. At Lone Star Geyser, about 5 km to the SSW of Old Faithful Geyser (Fig. 1), the volume of water flowing through outflow channels during nine eruptions in September 2010 varied between 15.4 m^3 and 28.1 m^3 with an average of 20.8 ± 4.1 m^3 (Karlstrom et al., 2013). At Steamboat Geyser in Norris Geyser Basin, measured volumes for three eruptions in 2000–2002 ranged between 130 m^3 and 246 m^3 (Friedman, 2007), for 29 eruptions in 2018–2020 ranged between 134 and 538 m^3 with a median of 351 m^3 (Reed et al., 2021), and 373 m^3 was recorded for a single eruption in September 2022 (Reed et al., 2024). The erupted volumes from Old Faithful Geyser are similar to those erupted from Lone Star Geyser but an order of magnitude less than those erupted at Steamboat Geyser. In the Valley of Geysers, Kamchatka, a chloride tracer method was used to estimate erupted volume of several geysers, with means of 23, 74 and 310 m^3 at Bolshoy, Velikan, and Grot Geysers, respectively (Kiryukhin et al., 2022). The very different methods used to estimate erupted volumes complicate comparison with these other geysers.

5.4. Solute mass discharge and transport

Based on five samples from the splash pool on the geyser cone (McCleskey et al., 2026), the highest-concentration solutes in the water erupted from Old Faithful Geyser are chloride (average of 425 $mg \cdot L^{-1}$), silica (SiO_2–349 $mg \cdot L^{-1}$), and sodium (346 $mg \cdot L^{-1}$). To calculate the annual mass discharge of solutes in water erupted by Old Faithful Geyser we multiply average solute concentrations in the five water samples from the splash pool (Fig. 3c) by the average volume of erupted water (26.3 m^3) (Table 1) and by the number of eruptions per year (5647), which is based on the average eruption interval of 93.1 min. We assume that solutes are not partitioned into the steam and remain in the liquid water.

Chloride discharge through the rivers draining the Yellowstone Plateau volcanic field is used as a proxy for heat flow from the magma-hydrothermal system (Hurwitz et al., 2012b). Fluoride is also of interest, because at relatively high concentrations in drinking water it can cause dental and skeletal fluorosis (Srivastava and Flora, 2020), and arsenic is a contaminant in surface and groundwaters and at high concentrations is a considerable public-health concern. Arsenic concentrations in Yellowstone's thermal waters are typically higher than drinking water standards (McCleskey et al., *2022a*). The average annual mass discharge of chloride, fluoride, and arsenic from Old Faithful is 63 tons, 3.9 tons and 241 kg, respectively (Table 3). The fraction of solutes discharged by the geyser is only a small fraction of the mass discharge in the Firehole River (Hurwitz et al., 2010; McCleskey et al., 2012). For example, chloride discharge from the geyser is only ~1% of the total discharge from the Upper Geyser Basin based on measurements made in 1966 and 1977 (Fournier et al., 1976).

To calculate the mass and volume of silica (SiO_2) precipitated on the geyser cone and along the outflow channels, we compare silica and chloride concentrations in the splash pool with concentrations of water in the outflow channels (Table 2). We multiply the ratio of median

Table 3
Solute concentrations and mass discharge from Old Faithful Geyser.

Sample[1]	Date	Cl^-	F	As	Cl[2]	F	As
		mg/L	mg/L	mg/L	ton/yr	ton/yr	kg/y
21WA128	9/5/2021	430	24.8	1.46	64	3.7	217
25WA111	4/14/2025	424	29.3	1.49	63	4.4	222
25WA112	4/15/2025	427	28.6	2.09	63	4.3	311
25WA118	6/26/2025	419	24.4	1.55	62	3.6	230
25WA115	7/12/2025	424	25.0	1.52	63	3.7	226
Average		**424.8**	**26.4**	**1.62**	**63**	**3.9**	**241**

1-Samples were collected from the splash pool on the Old Faithful Geyser Cone (Fig. 2).
2-Annual discharge is based on an average eruption interval of 93 min and average eruption volume of 26.3 m^3 which excludes the volume erupted as steam.

chloride concentration in the channels and the median concentration in the splash pool (1.15, section 4.1) by the median concentration of SiO_2 in the splash pool (354 mg·L^{-1}). This provides the expected SiO_2 concentrations at the end of the channels if it was as conservative as chloride. The calculated median SiO_2 concentration expected at the end of the channels (1.15 × 354 mg·L^{-1} = 405 mg·L^{-1}) is higher than the observed median concentration in the channels (356 mg·L^{-1}), implying that for every liter of water erupted, 49 mg of SiO_2 precipitates on the geyser cone and/or in the outflow channels. Based on the average annual average volume erupted of 1.49 × 10^5 m^3, which is the average eruption volume (26.3 m^3) multiplied by the number of eruptions per year (5647), we calculate that an average of 7 tons of SiO_2 are precipitated annually (Table 2).

5.5. Heat flow

We calculate the heat flow from eruptions of Old Faithful Geyser by assuming that the total mass of erupted water cools from 93 °C (boiling temperature at the local elevation) to ambient air, which at Yellowstone was ~1.3 °C on average between 1991 and 2020 (National Centers for Environmental Information, 2026) station USC00486845 at Old Faithful, Wyoming. We divide the total mass of liquid water erupted (25.3 × 10^3 kg) by the average eruption cycle (93 min) to get an average mass flow rate of 4.5 kg·sec^{-1}. To calculate the heat flow transported by liquid water, we multiply this flow rate by the liquid enthalpy (H) change in cooling from 93 °C (H = 390 kJ kg^{-1}) to 1.3 °C (H = 5.5 kJ kg^{-1}). The calculated heat transported by the liquid is thus 1.7 MW. To calculate the heat transported by steam mass fractions of 0.045 and 0.065 (section 5.2) that condense in the atmosphere, we multiply the latent heat of condensation of pure water (2270 kJ kg^{-1} at 93 °C) by the mass flow rate of steam (0.32 kg·sec^{-1} and 0.21 kg·sec^{-1} for steam mass fractions of 0.065 and 0.045, respectively). The heat transported by steam is 0.7 and 0.5 MW for mass fractions of 0.065 and 0.045, respectively. We neglect the contribution of kinetic energy of the jet in computing the energy budget because it accounts for ~1.5 kW which is less than 0.1% of the total heat flow from the geyser. The total heat flow from the geyser of 2.2 to 2.4 MW is significantly less than the 5.6 MW (1.34 × 10^6 cal·sec^{-1}) proposed by Rinehart (1980). This difference results from a different set of parameter values in the calculations, mainly a larger (and unconstrained) water volume and more frequent eruptions used by Rinehart (1980).

Heat flow has been estimated for a few other geysers and related thermal features in Yellowstone National Park. Heat flow at Lone Star Geyser is 1.5 MW (Karlstrom et al., 2013), an estimate that relies on an eruption volume that we noted is likely underestimated because it neglects evaporation losses. The heat flow from Doublet Pool, a non-erupting thermal feature, is 5.0 ± 0.2 MW (Liu et al., 2023). The calculated heat flow at Old Faithful Geyser is only a small fraction of the 4–8 GW from the Yellowstone caldera and its surroundings (Hurwitz et al., 2012b), but the localized heat output from the geyser is nevertheless very large. With an average continental heat flux of 0.07 W/m^2 (Davies and Davies, 2010; Lucazeau, 2019), heat flow from Old Faithful Geyser is equivalent to the heat loss through average continental crust over an area of 30–40 km^2.

5.6. Suggestions for future studies

The new dataset of water volume erupting from Old Faithful Geyser and its temporal variability provides a baseline for monitoring future changes in geyser activity that may result from varying climate, earthquakes, infrastructure development, and changes in heat flow from the underlying magmatic system. To improve the ability to track changes in the geyser's activity, some of the uncertainties associated with water volume measurements need to be reduced. Further, measurements are needed during different times of the day and during different seasons. In this study, based on several sampling campaigns, we showed that evaporation along the geyser's outflow channels is significant, and future studies would need to better quantify evaporation under different weather conditions. For comparison with other geysers in Yellowstone National Park and elsewhere around the world, there is a need to standardize methods for water-discharge measurement and heat flow calculations. Detailed documentation of the methods used to estimate volume and heat flow is needed. Finally, emerging technologies could possibly improve estimates of mass and/or volume discharge. These include the use of Uncrewed Aerial Systems (UAS) to acquire simultaneous optical and thermal infrared images (Müller et al., 2022) to better quantify steam and liquid flow rates during eruption, use of vortex flow meters (Fang et al., 2025) to measure the flow rate of steam, and deployment of high-temperature distributed temperature sensing (DTS) fiber optic cables (Khankishiyev et al., 2024) in the geyser conduit and outflow channels to capture spatial and temporal temperature variations.

6. Conclusions

Based on water-discharge measurements during 45 eruptions of Old Faithful Geyser in Yellowstone National Park, chemical analyses of erupted water, video analysis of the geyser jet, and thermodynamic calculations we conclude the following:

- The calculated average volume of water erupted by Old Faithful Geyser is 27.9 ± 9.4 m^3 which includes water discharge measured with a flume in an outflow channel, water flowing into the adjacent Firehole River measured by specific conductance, the volume of water that evaporates along the outflow channels between the geyser cone and the locations of discharge measurements, and the volume of water that erupts as steam.
- Estimates of erupted volume based on high-speed video recordings range from 21 to 30 m^3, with large uncertainties associated with fluid density and conduit geometry. The video recordings suggest that the volume of steam erupted during the liquid-dominated phase is negligible.
- There was no relation between geyser eruption volumes and the length of the preceding or following eruption intervals, but short eruptions resulted in smaller volumes. The lack of a relation between geyser eruption volumes and eruption intervals in the dataset might result from the large variation in the mass of water erupted as steam, in the amount of evaporation, and the accumulation of ice along the outflow channels, all which affect water-volume measurements.
- The average annual mass discharge of chloride, fluoride, and arsenic from Old Faithful is 63 tons, 3.9 tons, and 241 kg, respectively. The fraction of solutes discharged by the geyser is only a small fraction of the solute-mass discharge through the Firehole River.
- An average of 7 tons of SiO_2 are precipitated annually on the geyser cone and along the outflow channels. For calculated steam fractions of 4.5 to 6.5 wt%, the heat flow of the geyser is 2.2 to 2.4 MW.

The measurement and calculation methods used in this study provide a template for future studies quantifying eruption volumes at geysers worldwide. Data on erupted water volumes from Old Faithful, in addition to records of eruption intervals can provide the U.S. National Park Service with baseline information needed to better track changes in the geyser's activity. This in turn can inform the management of tourism around one of its most iconic resources (Foley et al., 2014).

CRediT authorship contribution statement

Shaul Hurwitz: Writing – original draft, Visualization, Validation, Resources, Project administration, Methodology, Investigation, Formal analysis, Data curation, Conceptualization. **R. Blaine McCleskey:** Writing – review & editing, Visualization, Validation, Resources, Methodology, Investigation, Formal analysis, Data curation, Conceptualization. **Maxwell L. Rudolph:** Writing – review & editing, Visualization, Validation, Software, Resources, Methodology, Investigation, Funding acquisition, Formal analysis, Data curation. **Sara Peek:** Writing – review & editing, Resources, Methodology, Investigation, Data curation. **David A. Roth:** Writing – review & editing, Methodology, Investigation. **Melissa Schott-Atkins:** Writing – review & editing, Investigation, Data curation. **Michael Manga:** Writing – review & editing, Validation, Supervision, Investigation, Funding acquisition, Conceptualization. **Kiernan F. Folz Donahue:** Writing – review & editing, Investigation. **Mara H. Reed:** Writing – review & editing, Investigation. **Jefferson D.G. Hungerford:** Writing – review & editing, Investigation.

Declaration of competing interest

The authors declare no conflicts of interest relevant to this study.

Acknowledgements

This study was conducted under research permit YELL-SCI- 08342. We thank Alison White from the Yellowstone Center for Resources research permit office for logistical support, Margery Price, Samantha Hilburn, and Tara Cross for help with measurements, and Rob Runkel, Katie Walton-Day, John Fulton, and David Susong for discussions and guidance with discharge measurements. We thank Steve Ingebritsen, Jean Vandemeulebrouck, and two anonymous reviewers for the constructive comments and suggestions. U.S. Geological Survey (USGS) participants were supported by the USGS Volcano Hazards Program and the Geothermal Research Investigations Project (GRIP). M. Rudolph was supported by NSF Grant EAR-2050352; M. Manga and M.H. Reed were supported by NSF Grant EAR-2116573. Any use of trade, firm, or product names is for descriptive purposes and does not imply endorsement by the U.S. Government.

Appendix A. Supplementary data

Supplementary data to this article can be found online at https://doi.org/10.1016/j.jvolgeores.2026.108624.

Data availability

Data presented in this study are available in U.S. Geological Survey data releases: McCleskey et al. (2022a) and McCleskey et al. (2026). Camera data are available on Zenodo (Rudolph, 2026).

References

Allen, E.T., Day, A.L., 1935. Hot Springs of the Yellowstone National Park. In: Carnegie Institute of Washington Publication, 466. Carnegie Institute, Troy, Mich, p. 525 pp.

Ardid, A., Vera, E., Kelly, C., Manga, M., Munoz-Saez, C., Maksymowicz, A., Ortega-Culaciati, F., 2019. Geometry of geyser plumbing inferred from ground deformation. J. Geophys. Res. 124, 1072–1083. https://doi.org/10.1029/2018JB016454.

Azzalini, A., Bowman, A.W., 1990. A look at some data on the old faithful geyser. J. R. Stat. Soc. Ser. C 39, 357–365. https://doi.org/10.2307/2347385.

Birch, F., Kennedy, G.C., 1972. Notes on geyser temperatures in Iceland and Yellowstone national park. Am. Geophys. Union Monogr. 16, 329–336. https://doi.org/10.1029/GM016p0329.

Bryan, T.S., 2008. The Geysers of Yellowstone Fourth Edition. Univ. Press of Colorado, Boulder, Colo.

Christiansen, R.L., 2001. The quaternary and Pliocene Yellowstone plateau volcanic field of Wyoming, Idaho, and Montana. U.S. Geol. Surv. Prof. Pap. 729-G, 145 pp. https://doi.org/10.3133/pp729G.

Cros, E., Roux, P., Vandemeulebrouck, J., Kedar, S., 2011. Locating hydrothermal acoustic sources at old faithful geyser using matched field processing. Geophys. J. Int. 187, 385–393. https://doi.org/10.1111/j.1365-246X.2011.05147.x.

Cullen, J.T., Hurwitz, S., Barnes, J.D., Lassiter, J.C., Penniston-Dorland, S., Kasemann, S. A., Thordsen, J.J., 2019. Temperature-dependent variations in mineralogy, major element chemistry and the stable isotopes of boron, lithium and chlorine resulting from hydration of rhyolite: constraints from hydrothermal experiments at 150 to 350 c and 25 MPa. Geochim. Cosmochim. Acta 261, 269–287. https://doi.org/10.1016/j.gca.2019.07.012.

Davies, J.H., Davies, D.R., 2010. Earth's surface heat flux. Solid. Earth 1, 5–24. https://doi.org/10.5194/se-1-5-2010.

Eibl, E.P., Müller, D., Walter, T.R., Allahbakhshi, M., Jousset, P., Hersir, G.P., Dahm, T., 2021. Eruptive cycle and bubble trap of Strokkur geyser, Iceland. J. Geophys. Res. 126. https://doi.org/10.1029/2020JB020769 p.e2020JB020769.

Eibl, E.P., Karmacharya, S., Shevchenko, A.V., Walter, T., Hersir, G.P., 2024. Video camera and seismic monitoring of water bulge explosion at Strokkur geyser, Iceland. Volcanica 7, 229–245. https://doi.org/10.30909/vol.07.01.229245.

Fagan, W.F., Swain, A., Banerjee, A., Ranade, H., Thompson, P., Staniczenko, P.P., Flynn, B., Hungerford, J., Hurwitz, S., 2022. Quantifying interdependencies in geyser eruptions at the upper geyser basin, Yellowstone National Park. J. Geophys. Res. 127. https://doi.org/10.1029/2021JB023749 p.e2021JB023749.

Fang, L., Zhang, X., Wang, Z., Zhao, D., Feng, Y., 2025. Research on steam flowrate measurement based on vortex uniform velocity tube integrated sensor. Flow Meas. Instrum. 103, 102854. https://doi.org/10.1016/j.flowmeasinst.2025.102854.

Fenner, C.N., 1936. Bore-hole investigations in Yellowstone Park. J. Geol. 44, 225–315. https://doi.org/10.1086/624425.

Foley, D., Fournier, R.O., Heasler, H.P., Hinckley, B., Ingebritsen, S.E., Lowenstern, J.B., Susong, D.D., 2014. Hydrogeology of the Old Faithful Area, Yellowstone National Park, Wyoming, and Its Relevance to Natural Resources and Infrastructure. US Geological Survey Open-File Report 2014-1058. https://doi.org/10.3133/ofr20141058.

Fournier, R.O., 1969. Old faithful: a physical model. Science 163, 304–305. https://doi.org/10.1126/science.163.3864.304.

Fournier, R.O., 1977. Chemical geothermometers and mixing models for geothermal systems. Geothermics 5, 41–50. https://doi.org/10.1016/0375-6505(77)90007-4.

Fournier, R.O., 1979a. A revised equation for the Na/K geothermometer. Geotherm. Res. Council Trans. 3, 221–224.

Fournier, R.O., 1979b. Geochemical and hydrologic considerations and the use of enthalpy-chloride diagrams in the prediction of underground conditions in hot-spring systems. J. Volcanol. Geotherm. Res. 5, 1–16. https://doi.org/10.1016/0377-0273(79)90029-5.

Fournier, R.O., Potter II, R.W., 1982. An equation correlating the solubility of quartz in water from 25 to 900 c at pressures up to 10,000 bars. Geochim. Cosmochim. Acta 46, 1969–1973. https://doi.org/10.1016/0016-7037(82)90135-1.

Fournier, R.O., White, D.E., Truesdell, A.H., 1976. Convective heat flow in Yellowstone National Park. In: Proceedings of the 2nd UN Symposium on the Development and Use of Geothermal Resources, San Francisco, pp. 731–739.

Friedman, I., 2007. Monitoring changes in geothermal activity at Norris geyser basin by satellite telemetry, Yellowstone National Park, Wyoming. In: Morgan, L.A. (Ed.), integrated Geoscience Studies in the Greater Yellowstone Area—Volcanic, Tectonic, and Hydrothermal Processes in the Yellowstone Geoecosystem, 1717. U.S. Geol. Surv. Prof. Pap, pp. 510–532. https://pubs.usgs.gov/pp/1717/downloads/pdf/p1717P.pdf.

Geis Jr., F., 1966. Old Faithful. Science 151, 223. https://doi.org/10.1126/science.151.3707.223.b.

Giggenbach, W.F., 1988. Geothermal solute equilibria. Derivation of Na-K-Mg-Ca geoindicators. Geochim. Cosmochim. Acta 52, 2749–2765. https://doi.org/10.1016/0016-7037(88)90143-3.

Hayden, F.V., 1883. A Report of Progress of the Exploration in Wyoming and Idaho for the Year 1878. *U.S. Geological and Geographical Survey of the Territories, 12th Annual Report, part II*, p. 503 p. https://doi.org/10.3133/70038941.

Hurwitz, S., Lowenstern, J.B., 2014. Dynamics of the Yellowstone hydrothermal system. Rev. Geophys. 52, 375–411. https://doi.org/10.1002/2014RG000452.

Hurwitz, S., Manga, M., 2017. The fascinating and complex dynamics of geyser eruptions. Annu. Rev. Earth Planet. Sci. 45, 31–59. https://doi.org/10.1146/annurev-earth-063016-015605.

Hurwitz, S., Shelly, D.R., 2017. Illuminating the voluminous subsurface structures of old faithful geyser, Yellowstone National Park. Geophys. Res. Lett. 44, 10–328. https://doi.org/10.1002/2017GL075833.

Hurwitz, S., Kumar, A., Taylor, R., Heasler, H., 2008. Climate-induced variations of geyser periodicity in Yellowstone National Park, USA. Geology 36, 451–454. https://doi.org/10.1130/G24723A.1.

Hurwitz, S., Evans, W.C., Lowenstern, J.B., 2010. River solute fluxes reflecting active hydrothermal chemical weathering of the Yellowstone plateau volcanic field, USA. Chem. Geol. 276, 331–343. https://doi.org/10.1016/j.chemgeo.2010.07.001.

Hurwitz, S., Hunt, A.G., Evans, W.C., 2012a. Temporal variations of geyser water chemistry in the upper geyser basin, Yellowstone National Park, USA. Geochem. Geophys. Geosyst. 13. https://doi.org/10.1029/2012GC004388.

Hurwitz, S., Harris, R.N., Werner, C.A., Murphy, F., 2012b. Heat flow in vapor dominated areas of the Yellowstone plateau volcanic field: implications for the thermal budget of the Yellowstone Caldera. J. Geophys. Res. 117 (B10). https://doi.org/10.1029/2012JB009463.

Hurwitz, S., Sohn, R.A., Luttrell, K., Manga, M., 2014. Triggering and modulation of geyser eruptions in Yellowstone National Park by earthquakes, earth tides, and weather. J. Geophys. Res. 119, 1718–1737. https://doi.org/10.1002/2013JB010803.

Hurwitz, S., Clor, L.E., McCleskey, R.B., Nordstrom, D.K., Hunt, A.G., Evans, W.C., 2016. Dissolved gases in hydrothermal (phreatic) and geyser eruptions at Yellowstone National Park, USA. Geology 44, 235–238. https://doi.org/10.1130/G37478.1.

Hurwitz, S., King, J.C., Pederson, G.T., Martin, J.T., Damby, D.E., Manga, M., Hungerford, J.D., Peek, S., 2020. Yellowstone's old faithful Geyser shut down by a severe thirteenth century drought. Geophys. Res. Lett. 47, e2020GL089871. https://doi.org/10.1029/2020GL089871.

Hurwitz, S., Manga, M., Campbell, K., Eibl, E., 2021. Why study geysers? Eos 102. https://doi.org/10.1029/2021EO161365.

Hurwitz, S., McCleskey, R.B., Jurgens, B.C., Lowenstern, J.B., Clor, L., Hunt, A.G., 2025. The systematics of stable hydrogen (δ^{2H}) and oxygen (δ^{18O}) isotopes and tritium (3H) in the hydrothermal system of the Yellowstone Plateau Volcanic Field, USA. Geochem. Geophys. Geosyst. 26, e2025GC012230. https://doi.org/10.1029/2025GC012230.

Hutchinson, R.A., Westphal, J.A., Kieffer, S.W., 1997. In situ observations of old faithful geyser. Geology 25, 875–878. https://doi.org/10.1130/0091-7613(1997)025<0875:ISOOOF>2.3.CO;2.

Jaworowski, C., Lynne, B.Y., Heasler, H., Foley, D., Smith, I.J., Smith, G.J., 2020. Detecting natural fractures with ground penetrating radar and airborne night-thermal infrared imagery around old faithful geyser, Yellowstone National Park, USA. Geothermics 85, 101775. https://doi.org/10.1016/j.geothermics.2019.101775.

Karlstrom, L., Hurwitz, S., Sohn, R., Vandemeulebrouck, J., Murphy, F., Rudolph, M.L., Johnston, M.J., Manga, M., McCleskey, R.B., 2013. Eruptions at lone star geyser, Yellowstone National Park, USA: 1. Energetics and eruption dynamics. J. Geophys. Res. 118, 4048–4062. https://doi.org/10.1002/jgrb.50251.

Kedar, S., Sturtevant, B., Kanamori, H., 1996. The origin of harmonic tremor at old faithful geyser. Nature 379, 708–711. https://doi.org/10.1038/379708a0.

Kedar, S., Kanamori, H., Sturtevant, B., 1998. Bubble collapse as the source of tremor at old faithful geyser. J. Geophys. Res. 103, 24283–24299. https://doi.org/10.1029/98JB01824.

Keller, L.M., Colman, D.R., Boyd, E.S., 2023. An active microbiome in old faithful geyser. PNAS Nexus 2, pgad066. https://doi.org/10.1093/pnasnexus/pgad066.

Khankishiyev, O., Salehi, S., Hasanov, G., Hu, Z., 2024. Application of distributed temperature sensing (DTS) in geothermal wells. In: Proceedings of the 49th Workshop on Geothermal Reservoir Engineering. Stanford University, Stanford, California. SGP-TR-227. https://www.proceedings.com/content/074/074051webtoc.pdf.

Kieffer, S.W., 1984. Seismicity at old faithful geyser: an isolated source of geothermal noise and possible analogue of volcanic seismicity. J. Volcanol. Geotherm. Res. 22, 59–95. https://doi.org/10.1016/0377-0273(84)90035-0.

Kieffer, S.W., 1989. Geologic nozzles. Rev. Geophys. 27, 3–38. https://doi.org/10.1029/RG027i001p00003.

Kieffer, S.W., 2017. Researching the earth—and a few of its neighbors. Annu. Rev. Earth Planet. Sci. 45, 1–29. https://doi.org/10.1146/annurev-earth-063016-020501.

Kilpatrick, F.A., Schneider, V.R., 1983. Use of flumes in measuring discharge. In: US Geological Survey Techniques of Water Resources Investigations. https://doi.org/10.3133/twri03A14, 03-A14.

King, J.M., Hurwitz, S., Lowenstern, J.B., Nordstrom, D.K., McCleskey, R.B., 2016. Multireaction equilibrium geothermometry: a sensitivity analysis using data from the lower geyser basin, Yellowstone National Park, USA. J. Volcanol. Geotherm. Res. 328, 105–114. https://doi.org/10.1016/j.jvolgeores.2016.10.010.

Kiryukhin, A.V., Polyakov, A.Y., Zhuravlev, N.B., Tsuchiya, N., Rychkova, T.V., Usacheva, O.O., Dubrovskaya, I.K., 2022. Dynamics of natural discharge of the hydrothermal system and geyser eruption regime in the valley of geysers, Kamchatka. Appl. Geochem. 136, 105166. https://doi.org/10.1016/j.apgeochem.2021.105166.

Liu, C.N., Lin, F.C., Manga, M., Farrell, J., Wu, S.M., Reed, M.H., Barth, A., Hungerford, J., White, E., 2023. Thumping cycle variations of doublet pool in Yellowstone National Park, USA. Geophys. Res. Lett. 50 (4). https://doi.org/10.1029/2022GL101175 p.e2022GL101175.

Lowenstern, J.B., Hurwitz, S., 2008. Monitoring a supervolcano in repose: heat and volatile flux at the Yellowstone Caldera. Elements 4, 35–40. https://doi.org/10.2113/GSELEMENTS.4.1.35.

Lu, X., Kieffer, S.W., 2009. Thermodynamics and mass transport in multicomponent, multiphase H_2O systems of planetary interest. Annu. Rev. Earth Planet. Sci. 37, 449–477. https://doi.org/10.1146/annurev.earth.031208.100109.

Lucazeau, F., 2019. Analysis and mapping of an updated terrestrial heat flow data set. Geochem. Geophys. Geosyst. 20, 4001–4024. https://doi.org/10.1029/2019GC008389.

Lynne, B.Y., Heasler, H., Jaworowski, C., Smith, G.J., Smith, I.J., Foley, D., 2018. Ground penetrating radar documents short-term near-surface hydrological changes around old faithful geyser, Yellowstone National Park, USA. J. Volcanol. Geotherm. Res. 354, 1–12. https://doi.org/10.1016/j.jvolgeores.2018.01.018.

Marler, G.D., 1951. Exchange of function as a cause of geyser irregularity [Wyoming]. Am. J. Sci. 249, 329–342.

Mastin, L.G., 1995. Thermodynamics of gas and steam-blast eruptions. Bull. Volcanol. 57, 85–98. https://doi.org/10.1007/BF00301399.

Matthews, N.E., Vazquez, J.A., Calvert, A.T., 2015. Age of the lava creek supereruption and magma chamber assembly at Yellowstone based on 40Ar/39Ar and U-P b dating of sanidine and zircon crystals. Geochem. Geophys. Geosyst. 16, 2508–2528. https://doi.org/10.1002/2015GC005881.

McCleskey, R.B., Clor, L.E., Lowenstern, J.B., Evans, W.C., Nordstrom, D.K., Heasler, H., Huebner, M.A., 2012. Solute and geothermal flux monitoring using electrical conductivity in the Madison, Firehole, and Gibbon rivers, Yellowstone National Park. Appl. Geochem. 27, 2370–2381. https://doi.org/10.1016/j.apgeochem.2012.07.019.

McCleskey, R.B., Nordstrom, D.K., Hurwitz, S., Colman, D.R., Roth, D.A., Johnson, M., Boyd, E.S., 2022. The source, fate, and transport of arsenic in the Yellowstone hydrothermal system-an overview. J. Volcanol. Geotherm. Res. 432, 107709. https://doi.org/10.1016/j.jvolgeores.2022.107709.

McCleskey, R.B., Roth, D.A., Hurwitz, S., Bliznik, P.A., Peek, S.E., Hunt, A.G., Repert, D. A., Nordstrom, D.K., Holloway, J.M., Ball, J.W., Price, M.B., 2022a. Water-Chemistry and Isotope Data for Selected Springs, Geysers, Streams, and Rivers in Yellowstone National Park, Wyoming (ver. 2.0, march 2025): U.S. Geological Survey Data Release. https://doi.org/10.5066/P92XKJU7.

McCleskey, R.B., Runkel, R.L., Murphy, S.F., Roth, D.A., 2025. Stream discharge determinations using slug additions and specific conductance. Water Resour. Res. 61, e2024WR037771. https://doi.org/10.1029/2024WR037771.

McCleskey, B., Peek, S., Hurwitz, S., Schott-Atkins, M., 2026. Flume Measurements of Water Erupted from Old Faithful Geyser. U.S. Geological Survey data release, Yellowstone National Park. https://doi.org/10.5066/P1YA3AJZ.

Müller, D., Walter, T.R., Zimmer, M., Gonzalez, G., 2022. Distribution, structural and hydrological control of the hot springs and geysers of El Tatio, Chile, revealed by optical and thermal infrared drone surveying. J. Volcanol. Geotherm. Res. 432, 107696. https://doi.org/10.1016/j.jvolgeores.2022.107696.

Munoz-Saez, C., Manga, M., Hurwitz, S., Rudolph, M.L., Namiki, A., Wang, C.Y., 2015. Dynamics within geyser conduits, and sensitivity to environmental perturbations: Insights from a periodic geyser in the El Tatio geyser field, Atacama Desert, Chile. J. Volcanol. Geotherm. Res. 292, 41–55. https://doi.org/10.1016/j.jvolgeores.2015.01.002.

National Centers for Environmental Information, 2026. Station USC00486845 at Old Faithful, Wyoming. https://www.ncdc.noaa.gov/cdo-web/datasets/GHCND/stations/GHCND:USC00486845/detail.

Nicholl, M.J., Wheatcraft, S.W., Tyler, S.W., Berkowitz, B., 1994. Is old faithful a strange attractor? J. Geophys. Res. 99, 4495–4503. https://doi.org/10.1029/93JB02575.

Nicholls, H.R., Rinehart, J.S., 1967. Geophysical study of geyser action in Yellowstone National Park. J. Geophys. Res. 72, 4651–4663. https://doi.org/10.1029/JZ072i018p04651.

NIST Standard Reference Database Number 69, 2025. doi:10.18434/T4D303.

O'Hara, K.D., Esawi, E.K., 2013. Model for the eruption of the old faithful geyser, Yellowstone National Park. GSA Today 23, 4–9. https://doi.org/10.1130/GSATG166A.1.

Paces, J.B., Hurwitz, S., Harrison, L.N., Lowenstern, J.B., McCleskey, R.B., 2024. Radiogenic strontium-and uranium-isotope tracers of water-rock interactions and hydrothermal flow in the Upper Geyser Basin, Yellowstone Plateau Volcanic Field, USA. Geochem. Geophys. Geosyst. 25, e2024GC011729. https://doi.org/10.1029/2024GC011729.

Parshall, R.L., 1950. Measuring Water in Irrigation Channels With Parshall Flumes and Small Weirs. United States Department of Agriculture, pp. 1–62. Circular 843.

Price, M.B., McCleskey, R.B., Oaks, A., Hurwitz, S., Nordstrom, D.K., 2024. Historic Water Chemistry Data for Thermal Features, Streams, and Rivers in the Yellowstone National Park Area, 1883–2021. U.S. Geological Survey data release. https://doi.org/10.5066/P9KSEVI1.

Reed, M.H., Munoz-Saez, C., Hajimirza, S., Wu, S.M., Barth, A., Girona, T., Rasht-Behesht, M., White, E.B., Karplus, M.S., Hurwitz, S., Manga, M., 2021. The 2018 reawakening and eruption dynamics of steamboat geyser, the worlds tallest active geyser. Proc. Natl. Acad. Sci. 118, e2020943118. https://doi.org/10.1073/pnas.2020943118.

Reed, M., Barth, A., Taira, T.A., Farrell, J., Manga, M., 2024. A shake and a surge: Assessing the possibility of an earthquake-triggered eruption at steamboat geyser. Volcanica 7, 733–748. https://doi.org/10.30909/vol.07.02.733748.

Rinehart, J.S., 1965. Earth tremors generated by old faithful geyser. Science 150, 494–496. https://doi.org/10.1126/science.150.3695.494.

Rinehart, J.S., 1969. Thermal and seismic indications of old faithful geyser's inner workings. J. Geophys. Res. 74, 566–573. https://doi.org/10.1029/JB074i002p00566.

Rinehart, J., 1980. Geysers and Geothermal Energy. Springer-Verlag, New York, p. 223. https://doi.org/10.1007/978-1-4612-6084-4.

Rojstaczer, S., Galloway, D.L., Ingebritsen, S.E., Rubin, D.M., 2003. Variability in geyser eruptive timing and its causes: Yellowstone National Park. Geophys. Res. Lett. 30. https://doi.org/10.1029/2003GL017853.

Rudolph, M.L., 2026. Video Recordings of Old Faithful Geyser. Zenodo. https://zenodo.org/records/17994407.

Rudolph, M.L., Sohn, R.A., 2017. A model for internal oscillations in geysers, with application to old faithful (Yellowstone, USA). J. Volcanol. Geotherm. Res. 343, 17–24. https://doi.org/10.1016/j.jvolgeores.2017.04.023.

Smith, I.J., Lynne, B.Y., Jaworowski, C., Qasim, I., Heasler, H., Foley, D., 2018. The formation of geyser eggs at old faithful geyser, Yellowstone national park, USA. Geothermics 75, 105–121. https://doi.org/10.1016/j.geothermics.2018.04.006.

Srivastava, S., Flora, S., 2020. Fluoride in drinking water and skeletal fluorosis: a review of the global impact. Curr. Environ. Health Rep. 7, 140–146. https://doi.org/10.1007/s40572-020-00270-9.

Teshima, N., Nishimura, T., 2024. Short-period flow oscillation during eruptions of Onikobe geyser, NE Japan: insights from thermal infrared observation and acoustic measurements. J. Volcanol. Geotherm. Res., 108092 https://doi.org/10.1016/j.jvolgeores.2024.108092.

The MathWorks Inc, 2025. 25.2.0.3150157 (R2025b). The MathWorks Inc, Natick, Massachusetts. https://www.mathworks.com.

Thiery, R., Mercury, L., 2009. Explosive properties of water in volcanic and hydrothermal systems. J. Geophys. Res. 114. https://doi.org/10.1029/2008JB005742.

U.S. Geological Survey, 2022. National Water Information System [Dataset]. U.S. Geological Survey Web Interface. Retrieved from https://nwis.waterdata.usgs.gov/nwis.

Van Orstrand, C.E., 1924. Temperatures in some springs and geysers in yellowstone national park. J. Geol. 32, 194–225 https://www.jstor.org/stable/30059934.

Vandemeulebrouck, J., Roux, P., Cros, E., 2013. The plumbing of old faithful geyser revealed by hydrothermal tremor. Geophys. Res. Lett. 40, 1989–1993. https://doi.org/10.1002/grl.50422.

Vicari, D., Van Dorp, J.R., 2013. On a bounded bimodal two-sided distribution fitted to the Old-Faithful geyser data. J. Appl. Stat. 40, 1965–1978. https://doi.org/10.1080/02664763.2013.800036.

Vitale, M.V., Gardner, P., Hinman, N.W., 2008. Surface water-groundwater interaction and chemistry in a mineral-armored hydrothermal outflow channel, Yellowstone National Park, USA. Hydrogeol. J. 16, 1381–1393. https://doi.org/10.1007/s10040-008-0344-8.

Wu, S.M., Ward, K.M., Farrell, J., Lin, F.C., Karplus, M., Smith, R.B., 2017. Anatomy of old faithful from subsurface seismic imaging of the Yellowstone Upper Geyser Basin. Geophys. Res. Lett. 44, 10–240. https://doi.org/10.1002/2017GL075255.

Wu, S.M., Lin, F.C., Farrell, J., Allam, A., 2019. Imaging the deep subsurface plumbing of old faithful geyser from low-frequency hydrothermal tremor migration. Geophys. Res. Lett. 46, 7315–7322. https://doi.org/10.1029/2018GL081771.